BRAIN PROCESSING

Cortical information flow during flexible sensorimotor decisions

Markus Siegel,[1,2]* Timothy J. Buschman,[2,3] Earl K. Miller[2]

During flexible behavior, multiple brain regions encode sensory inputs, the current task, and choices. It remains unclear how these signals evolve. We simultaneously recorded neuronal activity from six cortical regions [middle temporal area (MT), visual area four (V4), inferior temporal cortex (IT), lateral intraparietal area (LIP), prefrontal cortex (PFC), and frontal eye fields (FEF)] of monkeys reporting the color or motion of stimuli. After a transient bottom-up sweep, there was a top-down flow of sustained task information from frontoparietal to visual cortex. Sensory information flowed from visual to parietal and prefrontal cortex. Choice signals developed simultaneously in frontoparietal regions and travelled to FEF and sensory cortex. This suggests that flexible sensorimotor choices emerge in a frontoparietal network from the integration of opposite flows of sensory and task information.

Our reactions are not always the same to the same sensory input. Depending on context, we can map the same input onto different actions. This involves a distributed network of brain regions. During visuomotor decisions, choice predictive activity has been found in frontoparietal regions, including the lateral intraparietal area (LIP) (*1*–*4*), prefrontal cortex (PFC) (*1*, *5*–*9*), frontal eye fields (FEF) (*7*), and motor and sensory cortex (*10*–*13*). However, it remains unclear how choice signals evolve. Do they flow bottom-up, flow top-down, or evolve concurrently across brain regions? Do choice signals in sensory regions reflect their causal effect on the decisions or feedback from decision stages (*12*)? Similarly, little is known about the flow of task signals. Neuronal activity encodes task rules in prefrontal (*6*, *8*, *14*, *15*), parietal (*2*), and visual (*16*) cortices. Task-dependent attention modulates neuronal activity throughout sensory cortices (*17*–*19*). It remains unknown how task signals evolve across these regions.

We trained two monkeys on a flexible visuomotor task (Fig. 1 and materials and methods). They categorized either the color (red versus green) or the direction (up versus down) of a colored visual motion stimulus, reporting it with a left or right saccade (Fig. 1A). A visual cue instructed animals about the task (motion or color, Fig. 1C). Each task was indicated by two different visual cues to dissociate cue and task-related activity. Color and motion spanned a broad range around the category boundaries (yellow and horizontal) (Fig. 1B and fig. S1). Both monkeys were proficient at categorizing the cued feature (Fig. 1D) (94% and 89% correct for motion and color tasks, respectively, excluding ambiguous trials with stimuli on the category boundary).

[1]Centre for Integrative Neuroscience and MEG Center, University of Tübingen, Tübingen, Germany. [2]Picower Institute for Learning and Memory and Department of Brain and Cognitive Sciences, Massachusetts Institute of Technology, Cambridge, MA 02139, USA. [3]Princeton Neuroscience Institute and Department of Psychology, Princeton University, Princeton, NJ 08544, USA.
*Corresponding author. E-mail: markus.siegel@uni-tuebingen.de

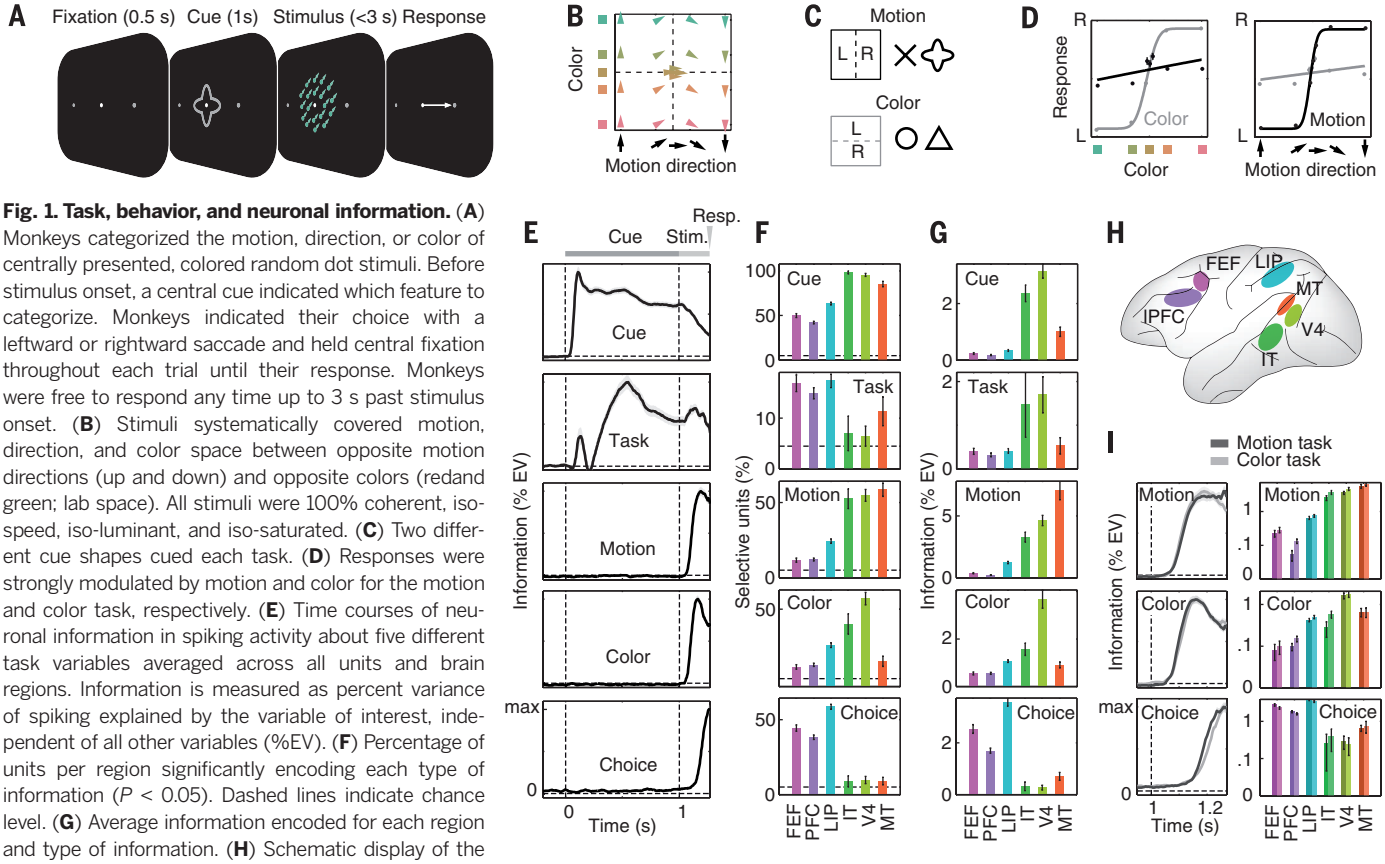

Fig. 1. Task, behavior, and neuronal information. (**A**) Monkeys categorized the motion, direction, or color of centrally presented, colored random dot stimuli. Before stimulus onset, a central cue indicated which feature to categorize. Monkeys indicated their choice with a leftward or rightward saccade and held central fixation throughout each trial until their response. Monkeys were free to respond any time up to 3 s past stimulus onset. (**B**) Stimuli systematically covered motion, direction, and color space between opposite motion directions (up and down) and opposite colors (redand green; lab space). All stimuli were 100% coherent, iso-speed, iso-luminant, and iso-saturated. (**C**) Two different cue shapes cued each task. (**D**) Responses were strongly modulated by motion and color for the motion and color task, respectively. (**E**) Time courses of neuronal information in spiking activity about five different task variables averaged across all units and brain regions. Information is measured as percent variance of spiking explained by the variable of interest, independent of all other variables (%EV). (**F**) Percentage of units per region significantly encoding each type of information ($P < 0.05$). Dashed lines indicate chance level. (**G**) Average information encoded for each region and type of information. (**H**) Schematic display of the recorded brain regions. lPFC, lateral prefrontal cortex. (**I**) Time course of average motion, color, and choice information analyzed separately for motion and color categorization tasks. Information is log-scaled to facilitate comparison between tasks. All error bars denote SEM.

We recorded multi-unit activity (MUA) from up to 108 electrodes simultaneously implanted in six cortical regions acutely each day (Fig. 1H and materials and methods): FEF (532), dorsolateral PFC (1020), LIP (807), IT (57), V4 (155), and MT (123) (total of 2694 multi-units). For each multi-unit, we quantified how neural activity encoded cue identity, task (motion versus color), stimulus motion direction, stimulus color, and motor choice. Information was quantified as spiking variance across trials explained by each factor. All five types of information were quantified independently; for example, choice measured only information about the choice that was not explained by cue, task, color, or motion (see materials and methods). To rule out activity due to the saccade itself, we included neuronal activity up to 5 ms before saccade onset.

Averaging across all units revealed temporal dynamics of information (Fig. 1E). Cue information peaked directly after cue onset and stayed tonically elevated during cue presentation (latency to reach half maximum: 74 ± 1 ms SE). Task information showed a bimodal dynamic. A transient peak shortly after cue onset had a similar latency as cue information (100 ± 25 ms). This transient peak was followed by a dip and later rise of sustained task information (333 ± 15 ms). In contrast to cue information, task information increased during stimulus presentation. Motion and color information rose after stimulus onset with a significantly shorter latency for color (98 ± 2 ms) as compared with motion (108 ± 2 ms) information ($P < 0.001$). Last, choice information rose (193 ± 1 ms) before the motor responses (270 ms ± 3 ms) and significantly later than motion and color information (both $P < 0.0001$).

We quantified for each type of information the percentage of units with significant effects (Fig. 1F) and the average amount of information (Fig. 1G). We used the second half of the cue interval (0.5 to 1 s) for cue and task information, the interval from stimulus onset to the average response latency (1 to 1.270 s) for motion and color information, and the 200-ms interval preceding the saccade for choice information. We found significant encoding of each type of information in each region ($P < 0.05$ for all regions and information), but the regional profiles differed. In accordance with shape selectivity of V4 and IT, we found the most frequent and strongest cue information there. Task selectivity was frequent in all regions and strongest in V4 and IT. Motion and color information were strongest in MT and V4, respectively. Choice information was most frequent and strongest in LIP, FEF, and PFC. Task (motion versus color) had little effect on strength and dynamics of motion, color, and choice information (Fig. 1I) (*20*, *21*). There was no evidence that only task-relevant sensory information was routed to frontoparietal stages and no evidence that choice information was present only in the task-relevant sensory region. In sum, all types of information were encoded across the entire visuomotor pathway, albeit with different incidences and strength.

Next, we investigated the temporal dynamics of information across regions. Cue information flowed bottom-up, rising first in MT, followed by LIP, V4, IT, FEF, and PFC (Fig. 2A). Most of the pairwise comparisons revealed significant latency differences between regions (Fig. 2B, $P < 0.001$). Task information showed very different dynamics (Fig. 2C). There was a significant early transient peak of task information (<150 ms) in IT and V4 only, without a latency difference between V4 and IT ($P > 0.05$). The latency of this peak in IT (72 ms) was not different ($P > 0.05$) from the latency of cue information in IT (also 72 ms). In V4, the transient peak of task information was slightly later (96 ms) than cue information (73 ms) ($P < 0.05$). Directly after this transient peak, task information was low in the PFC, but then appeared there first and flowed

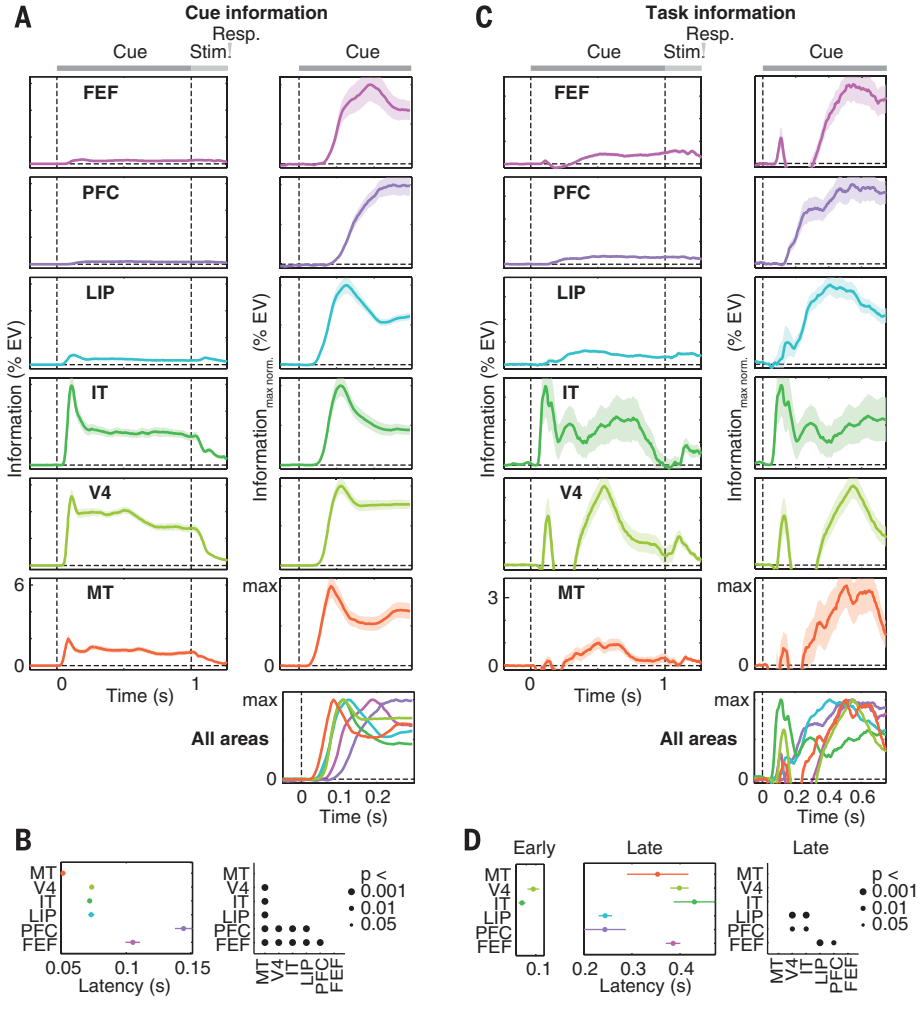

Fig. 2. Dynamics of cue and task information. (**A**) Each row displays for one brain region the average time course of neuronal information about cue identity. Left graphs display raw information (% EV, same scale for all regions). To support comparison across regions, right graphs display time courses normalized by maximum information for the interval of interest. The bottom right graph shows an overlay of all regions' information time courses. Cue and stimulus onsets are at time = 0 s and time = 1 s, respectively. (**B**) Comparison of cue information latencies between regions. Latencies are quantified as the time to reach half maximum information. Black dots in the right graph indicate significant latency differences between regions. (**C**) Time courses of task information across regions. Same conventions as in (A). (**D**) Comparison of task information latencies between regions. Latencies were separately analyzed for the early transient peak around 100 ms and for the later sustained increase of task information after 200 ms. Early peak latencies were only estimated for regions that showed a significant effect (V4 and IT, $P < 0.05$). Same conventions as in (B). All error bars denote SEM.

from PFC to LIP, MT, FEF, V4, and IT. Many pairwise latency comparisons were significant according to this pattern (Fig. 2D, $P < 0.01$). In particular, task information rose earlier in PFC and LIP than in FEF, V4, and IT (all $P < 0.01$). In summary, IT and V4 first extracted task information from the cues along with the encoding of cue identity. After this transient burst, there was a flow of sustained task information from PFC and LIP across the entire sensorimotor hierarchy.

Motion information rose first in MT, followed by LIP, V4, IT, FEF, and PFC (Fig. 3A). Color information rose first in MT, followed by V4, LIP, FEF, IT, and PFC (Fig. 3C). Most pairwise comparisons revealed latency differences between regions according to these sequences (Fig. 3, B and D, $P < 0.05$). Furthermore, color information appeared significantly earlier than motion information in V4, MT, PFC, and FEF (all $P < 0.001$). Analyzing motion and color tasks individually confirmed these results and showed that neuronal latencies for motion and color information were almost identical for both tasks (fig. S2).

Choice signals had a different dynamic. If spontaneous fluctuations of activity influenced animals' choices, activity would predict the choice even before presentation of the motion-color stimulus. Indeed, for all regions except IT, significant choice information preceded stimulus onset (–0.5 to 1 s, $P < 0.01$). We ruled out that this prestimulus choice information merely reflected an effect of the previous trial (see materials and methods). We next investigated the build-up of choice information during decisions (Fig. 4). Because this reflects the forthcoming behavioral response, we time-locked analysis to the saccade. Choice information increased in LIP and PFC before FEF (Fig. 4B, $P < 0.05$), but there was no latency difference between LIP and PFC. Choice information increased later in V4 and MT than in LIP and PFC (Fig. 4B, all $P < 0.05$), suggesting feedback of choices from frontoparietal stages. Analyzing choice information for motion and color tasks individually confirmed the above results (fig. S3).

Our results provide insights into the neuronal mechanisms underlying sensorimotor choices (summarized in fig. S4). First, sensory (cue, motion, or color), cognitive (task), and behavioral (choice) information was not confined to specific cortical regions but instead broadly distributed. This is incompatible with models of compartmentalized cortical function. Our results instead suggest a graded functional specialization of cortical regions with information shared between regions (*22*). Second, sensory information flowed feed-forward from sensory cortex. Third, task information was first extracted in an early, transient burst in higher sensory cortex (V4 and IT). This early transient may reflect the learned cue associations, that is, the grouping of the two cues for each task into one representation that is then fed forward to PFC and LIP. After the early transient, sustained task information appeared first in PFC and LIP and then spread to other regions. Thus, task information may need to reach PFC and LIP before being broadcast across the

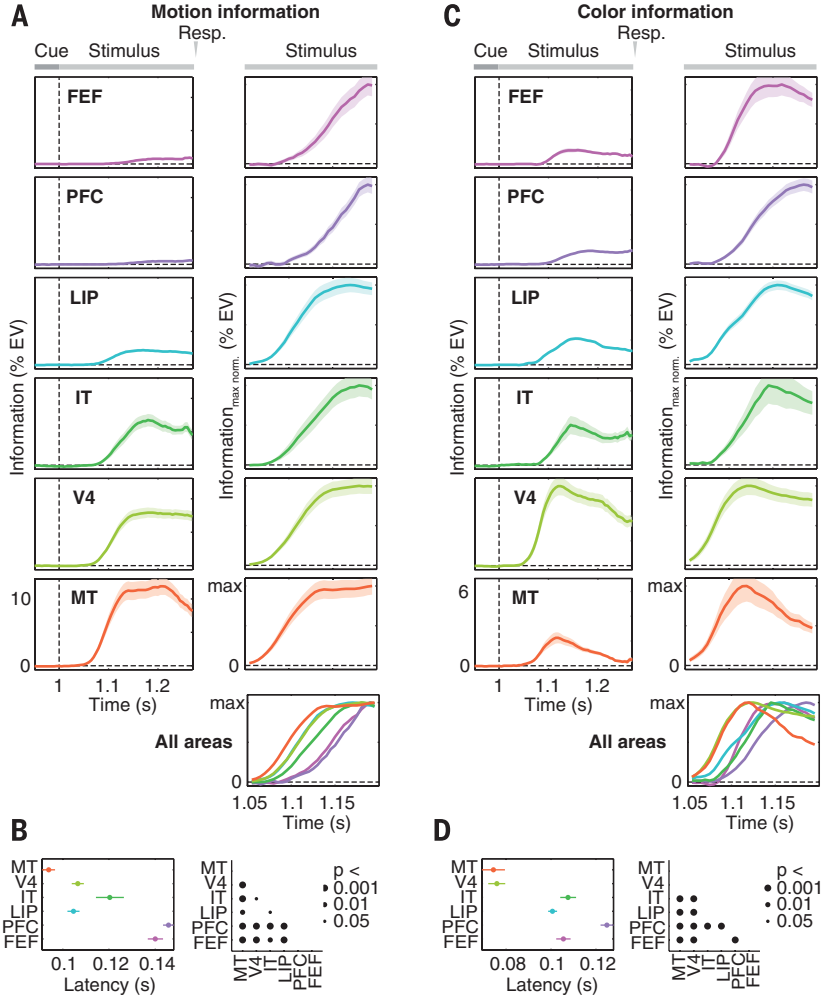

Fig. 3. Dynamics of motion and color information. Time courses and latencies of neuronal information about (**A** and **B**) motion direction and (**C** and **D**) color of the categorized stimulus. Stimulus onset is at time = 1 s. All other conventions as in Fig. 2.

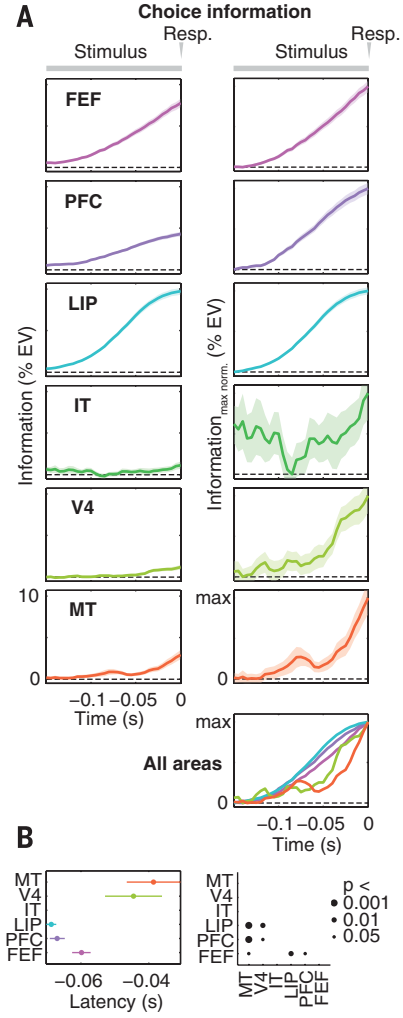

Fig. 4. Dynamics of choice information. Response-locked (**A**) time courses and (**B**) latencies of neuronal information about the animals' choice. Responses are at time = 0 s. Latency was not estimated for IT because there was no significant increase of choice information in IT in the analyzed interval (linear regression, $P > 0.05$). All other conventions as in Figs. 2 and 3.

sensorimotor pathway (*23*). Fourth, choice predictive activity was present in sensory (V4 and MT), frontoparietal (LIP and PFC), and premotor (FEF) cortex before onset of the decision process. This suggests a link between spontaneous fluctuations of neuronal activity along the entire sensorimotor pathway and subsequent decisions. Fifth, choice signals first and simultaneously built up in PFC and LIP and then followed in FEF. Our findings accord with previous reports of ramping choice predictive activity in LIP (*3*), PFC (*7*), and FEF (*7*) but shed light on how choices are made in this network. Our results suggest that, although sensory information reaches LIP and FEF before PFC, the accumulation of sensory evidence occurs first and jointly in LIP and PFC before decision signals are relayed to FEF. Similar dynamics in PFC and LIP could indicate that accumulation of sensory evidence depends on their recurrent interactions (*24*, *25*). The delayed choice signals in FEF may reflect the transformation of accumulated evidence into a discrete choice (*26*). Sixth, we found an increase of choice signals in LIP and PFC before MT and V4. This is consistent with feedback of choice signals from frontoparietal to sensory cortex (*12*, *13*, *27*). This may support cooperative computations between different hierarchical stages (*28*) and perceptual stability (*27*). In sum, flexible sensorimotor decisions are not a simple feed-forward process but result from complex temporal dynamics, including feed-forward and feedback interactions between frontal and posterior cortex.

REFERENCES AND NOTES

1. D. A. Crowe *et al.*, *Nat. Neurosci.* **16**, 1484–1491 (2013).
2. S. J. Goodwin, R. K. Blackman, S. Sakellaridi, M. V. Chafee, *J. Neurosci.* **32**, 3499–3515 (2012).
3. M. N. Shadlen, W. T. Newsome, *Proc. Natl. Acad. Sci. U.S.A.* **93**, 628–633 (1996).
4. D. J. Freedman, J. A. Assad, *Nature* **443**, 85–88 (2006).
5. C. H. Donahue, D. Lee, *Nat. Neurosci.* **18**, 295–301 (2015).
6. M. G. Stokes *et al.*, *Neuron* **78**, 364–375 (2013).
7. J. N. Kim, M. N. Shadlen, *Nat. Neurosci.* **2**, 176–185 (1999).
8. K. Merten, A. Nieder, *Proc. Natl. Acad. Sci. U.S.A.* **109**, 6289–6294 (2012).
9. D. J. Freedman, M. Riesenhuber, T. Poggio, E. K. Miller, *Science* **291**, 312–316 (2001).
10. T. H. Donner, M. Siegel, P. Fries, A. K. Engel, *Curr. Biol.* **19**, 1581–1585 (2009).
11. K. H. Britten, W. T. Newsome, M. N. Shadlen, S. Celebrini, J. A. Movshon, *Vis. Neurosci.* **13**, 87–100 (1996).
12. H. Nienborg, B. G. Cumming, *Nature* **459**, 89–92 (2009).
13. N. K. Logothetis, J. D. Schall, *Science* **245**, 761–763 (1989).
14. J. D. Wallis, K. C. Anderson, E. K. Miller, *Nature* **411**, 953–956 (2001).
15. K. Johnston, H. M. Levin, M. J. Koval, S. Everling, *Neuron* **53**, 453–462 (2007).
16. R. Muhammad, J. D. Wallis, E. K. Miller, *J. Cogn. Neurosci.* **18**, 974–989 (2006).
17. R. Desimone, J. Duncan, *Annu. Rev. Neurosci.* **18**, 193–222 (1995).
18. S. Kastner, L. G. Ungerleider, *Annu. Rev. Neurosci.* **23**, 315–341 (2000).
19. J. H. Reynolds, L. Chelazzi, *Annu. Rev. Neurosci.* **27**, 611–647 (2004).
20. V. Mante, D. Sussillo, K. V. Shenoy, W. T. Newsome, *Nature* **503**, 78–84 (2013).
21. J. Duncan, *J. Exp. Psychol. Gen.* **113**, 501–517 (1984).
22. W. Singer, *Trends Cogn. Sci.* **17**, 616–626 (2013).
23. E. K. Miller, J. D. Cohen, *Annu. Rev. Neurosci.* **24**, 167–202 (2001).
24. M. Siegel, T. H. Donner, A. K. Engel, *Nat. Rev. Neurosci.* **13**, 121–134 (2012).
25. X. J. Wang, *Neuron* **60**, 215–234 (2008).
26. T. D. Hanks *et al.*, *Nature* **520**, 220–223 (2015).
27. K. Wimmer *et al.*, *Nat. Commun.* **6**, 6177 (2015).
28. M. Siegel, K. P. Körding, P. König, *J. Comput. Neurosci.* **8**, 161–173 (2000).

ACKNOWLEDGMENTS

We thank J. Roy, C. von Nicolai, and J. Hipp for helpful discussions. This work was supported by National Institute for Mental Health (NIMH) grant 5R37MH087027 (E.K.M.), MIT Picower Innovation Fund (E.K.M.), National Institutes of Health (NIH) grant R00 MH092715 (T.J.B.), and the Centre for Integrative Neuroscience (Deutsche Forschungsgemeinschaft, EXC 307) (M.S.). All behavioral and electrophysiological data are archived at the Centre for Integrative Neuroscience, University of Tübingen, Germany.

SUPPLEMENTARY MATERIALS

www.sciencemag.org/content/348/6241/1352/suppl/DC1
Materials and Methods
Figs. S1 to S4
References (*29*–*35*)

4 March 2015; accepted 8 May 2015
10.1126/science.aab0551

COMETARY NUCLEI

The shape and structure of cometary nuclei as a result of low-velocity accretion

M. Jutzi[1]* and E. Asphaug[2]

Cometary nuclei imaged from flyby and rendezvous spacecraft show common evidence of layered structures and bilobed shapes. But how and when these features formed is much debated, with distinct implications for solar system formation, dynamics, and geology. We show that these features could be a direct result of accretionary collisions, based on three-dimensional impact simulations using realistic constitutive properties. We identify two regimes of interest: layer-forming splats and mergers resulting in bilobed shapes. For bodies with low tensile strength, our results can explain key morphologies of cometary nuclei, as well as their low bulk densities. This advances the hypothesis that nuclei formed by collisional coagulation—either out of cometesimals accreting in the early solar system or, alternatively, out of comparable-sized debris clumps paired in the aftermath of major collisions.

Comets or their precursors formed in the outer planets region, possibly millions of years before planet formation. Cometary nuclei may be fluffy condensates (*1*) or rubble piles (*2*) assembled by hierarchical accretion (*3*). Alternatively, they may be relics of catastrophically disrupted progenitors (*4*). Whether their interior structures preserve a record of their original accumulation is much debated (*5*, *6*), as is their geophysical connection to the Kuiper belt objects (KBOs) that are the likely source (*7*) of 1P/Halley and Jupiter family comets (JFCs)—all of the comets visited by spacecraft to date. Models of present-day dynamical evolution (*4*) suggest that KBOs smaller than ~5 km in diameter have catastrophic disruption lifetimes shorter than the age of the solar system, in which case JFCs, even if delivered as intact KBOs, are unlikely to be primordial. Others (*8*) argue that KBOs larger than ~60 km grew by efficient hierarchical accretion, whereas KBOs smaller than ~4 km probably survived as primordial relics. Models based on gravitational instability along with particle clumping in turbulent flows predict that asteroids and comets were born big (*9*, *10*) and bypassed the primary accretion phase of kilometer-sized bodies entirely. If so, then JFCs are secondary collisional relics from KBO-scale collisions (*11*, *12*). Dynamics is part of the story, chemistry another: In a thermodynamic sense, JFCs are highly primitive. The supervolatiles driving cometary activity and disruption (*6*) require there to have been minimal processing by internal heating and differentiation inside of a parent body and minimal shock heating by energetic impacts.

Whatever their origin, cometary nuclei come apart easily due to tides (*13*) and other gentle stresses (*14*). They are weakly consolidated at scales ~100 m or less (*13*). Estimated and measured bulk densities are half that of water ice, requiring considerable porosity. These data and other crucial information are obtained from astronomical observations and theoretical interpretations (*5*, *13*), flyby missions (*15*, *16*), and the European Space Agency's Rosetta rendezvous mission to 67P/Churyumov-Gerasimenko (*17*). Here we focus on the topographic and structural expressions of cometary nuclei identified by spacecraft.

There are two structural clues to cometary origin. First, there is a clear record of layers (*18*, *19*) in 9P/Tempel 1 and 67P/C-G and possibly also in 19P/Borrelly and 81P/Wild 2. The layers of 67P

[1]Physics Institute, Space Research and Planetary Sciences, Center for Space and Habitability, University of Bern, Sidlerstrassse 5, 3012 Bern, Switzerland. [2]School of Earth and Space Exploration, Arizona State University, PO Box 876004, Tempe, AZ 85287, USA.
*Corresponding author. E-mail: martin.jutzi@space.unibe.ch

www.sciencemag.org/content/348/6241/1352/suppl/DC1

Supplementary Material for

Cortical information flow during flexible sensorimotor decisions

Markus Siegel,* Timothy J. Buschman, Earl K. Miller

*Corresponding author. E-mail: markus.siegel@uni-tuebingen.de

Published 19 June 2015, *Science* **348**, 1352 (2015)
DOI: 10.1126/science.aab0551

This PDF file includes:

Materials and Methods

Subjects and recordings

Experiments were performed in two rhesus monkeys (one male, one female). All procedures followed the guidelines of the Massachusetts Institute of Technology Committee on Animal Care and the National Institutes of Health. Each monkey was implanted with a titanium head bolt to immobilize the head. Following the behavioral training, three titanium recording chambers were stereotactically implanted over frontal, parietal, and occipitotemporal cortices in the left hemisphere. Through these chambers, we simultaneously implanted Epoxy-coated tungsten electrodes in the lateral prefrontal cortex, frontal eye fields, lateral intraparietal cortex, inferotemporal cortex (TEO), visual area V4, and the middle temporal area (MT). Electrodes were lowered using custom-built microdrive assemblies that lowered electrodes in pairs or triplets from a single screw. These microdrive assemblies were designed for a high density of electrodes (1 mm spacing for pairs or 0.7 mm triangular spacing for triples) to maximize the number of simultaneously recorded neural signals across the six regions of interest. The electrodes were acutely lowered through the intact dura at the beginning of every recording session. Electrodes were simultaneously advanced in pairs or triplets of electrodes with penetrations typically angled relative to the cortical surface. We did not aim for a specific layer or fine-tune the positioning for specific cells. Thus, recordings were from all cortical layers with no bias for a specific depth. Electrodes were allowed to settle for a minimum of 1 h before recording. After each recording session, electrodes were retracted and the microdrive assemblies were removed from the recording chambers.

Neuronal activity was recorded across a maximum of 108 electrodes simultaneously. All signals were referenced to ground and recorded broad-band at 40 kHz. Offline, we extracted the continuous time-course of multi-unit spiking activity (MUA by filtering the broad-band signal between 500 Hz and 6 kHz (2^{nd}-order zero-phase forward-reverse Butterworth filter), rectification, low-pass filtering at 250 Hz (2^{nd}-order zero-phase forward-reverse Butterworth filter), and resampling at 1 kHz (*29*, *30*).

Behavioral Task

Monkeys were trained on a flexible visuomotor decision making task. All stimuli were displayed on a color calibrated CRT monitor at 100 Hz vertical refresh rate. An infrared-based eye-tracking system continuously monitored eye position at 240 Hz. Behavioral control of the behavioral task was handled by the Monkeylogic program (www.monkeylogic.net) (*31*, *32*).

Each trial was initiated when the animal fixated on a point at the center of the screen. Fixation was required within 1.2° of visual angle of the fixation point. After a short fixation period (500 ms), the animal was presented with a visual task cue for 1000 ms. Cues were four different gray shapes (Fig. 1C) of about 1.5° visual angle diameter that were presented centrally on the fixation spot. Two of the four shapes cued the motion and color task, respectively (Fig. 1C). Using two cues for each task allowed us to dissociate neuronal information about the cue (the visual shape of the cue) and neuronal information about the task at hand (motion vs. color).

After the cue period, the cue was switched off and a stimulus was presented centrally on the fixation spot. Stimuli were colored dynamic random dot patterns with 100% motion coherence presented centrally on the fixation spot (stimulus diameter : 3.2°; dot diameter: 0.08°; number of dots: 400; dot speed: 1.67°/s or 10°/s for half of the recording sessions, respectively). To prevent learning of dot patterns, new stimuli were generated for each recording session. To rule out effects of stimulus variability on neuronal choice information, the same stimulus (dot pattern) was used for all trials per recording session. On each trial, all dots moved in the same direction and had the same color. There were 7 possible stimulus colors and 7 possible motion directions. Colors and motion directions were chosen to optimize perceptual equidistance and equivalence within and between feature dimensions (Fig. S1). 4 motion directions spanned the range between upward (90º) and downward (-90º) motion through rightward motion (0º) in 60º steps (-90º, -30º, 30º, 90º). In addition, 3 motion directions were placed on (0º) and near (-5º, 5º) the category boundary (right). Similarly, 4 colors spanned the range between red (90º) and green (-90º) through yellow (0º) in 60º steps (-90º, -30º, 30º, 90º). In addition, 3 colors were placed on (0º) and near (-5º, 5º) the category boundary (yellow). To optimize perceptual homogeneity, all colors were defined in the CIE L*a*b* space and had the same luminance and saturation.

Depending on the task cued at the beginning of each trial, the animals categorized either the color (red vs. green) or motion direction (up vs. down) of the stimulus and reported their percept with a left or right saccade. The stimulus-response mapping for each task was fixed (Fig. 1C). Two saccade targets were displayed 6º to the left and right of the fixation spot throughout the trial. Animals had to respond with one direct saccade to one of these targets. Animals were free to respond at any time up to 1s after stimulus onset (Fig. 1A). For correct responses, animals were rewarded with apple juice. Animals were always rewarded for ambiguous trials with stimuli on the category boundary (yellow and right for color and motion task, respectively). These ambiguous trials were excluded for calculating the animals' percent correct performance.

Recording locations

We recorded multi-unit spiking activity (MUA) from a total of 2694 recording sites (1753 and 941 for the two monkeys) in 48 recording sessions (31 and 17 for the two monkeys) across all six investigated regions: FEF: 532 sites, dlPFC: 1020 sites, LIP: 807 sites, IT: 57 sites, V4: 155 sites, MT: 123 sites. We recorded from up to 108 electrodes simultaneously per session (mean/STD: 56/17 electrodes). For each session, we recorded at least from three regions simultaneously. Across all sessions, all pairs of regions were at least once recorded simultaneously.

Recordings were performed through three recording chambers that were stereotactically placed over frontal (FEF and PFC recordings), parietal (LIP recordings), and occipitotemporal (MT, V4 and IT recordings) cortex according to detailed 3D planning using custom MATLAB software and based on high-resolution structural MRIs of each animal. Frontal, parietal and occipitotemporal recording chambers were placed about 28 mm anterior, 2 mm posterior, and 1 mm posterior to the interaural plane, respectively.

The area definition of each recording site was based on the stereotactic recording location, on neuronal responses in a functional mapping task, and on microstimulation results. To this end, before recording the main task, we functionally characterized recording locations in several recording sessions during passive fixation with manually controlled visual stimuli and automatically flashed colored dynamic random dot patterns. Furthermore, on each recording session and in addition to the main task, the animals performed a functional mapping task. During central fixation, brief (150 ms) dynamic random dot patterns of different motion directions and colors were passively flashed on the fixation spot. Stimulus parameters were identical to the stimuli used during the main task. Motion directions and colors spanned the entire direction and hue space with 30º spacing. These stimuli were used to characterize the visual responsiveness and tuning of the recorded spiking activity. Following the flashed stimuli and a brief delay, a brief (100 ms) spot of light was flashed at one out of six different locations in the periphery. After a memory delay (750 ms), the fixation point was extinguished and the animal made a saccade to the remembered location of the light spot. This delayed saccade task was used to isolate LIP from surrounding regions, as it is the only region in the parietal cortex that shows spatially selective memory delay activity (*33*). Recording sites in the lateral bank of the intraparietal sulcus with significant spatially selective memory delay activity ($p < 0.05$) and/or significant ($p < 0.05$) visual responses to the random dot patterns in the functional mapping task were classified as LIP.

We used microstimulation to demarcate FEF from dlPFC in the frontal recording chamber. An isolated pulse stimulator was used for electrical stimulation. Stimulation was delivered as a 200 ms train of biphasic pulses with a width 400 μs and an pulse frequency of 330 Hz. Stimulation was performed using the same electrodes as for recording. Stimulation current

was started at 150 μA and reduced to find the threshold at which an eye movement vector was elicited 50% of the time. Sites that had thresholds of stimulation amplitudes <50 μA were classified as FEF (*34*). Anterior sites were classified as lPFC.

Occipitotemporal recording sites were classified as MT, V4 and TEO based on their anatomical location and if they showed significant ($p < 0.05$) visual responses to the random dot patterns in the functional mapping task. MT recordings sites were in the lower and medial bank of the posterior third of the superior temporal sulcus. V4 recording sites were posterior and ventral to MT sites on the angular gyrus. TEO recording sites were on the lateral convexity of the inferior temporal gyrus between the ascending part of the inferior occipital sulcus and the posterior middle temporal sulcus.

Information encoded by neuronal spiking activity

We quantified the information encoded by multi-unit spiking activity (MUA) about several task factors. Specifically, we used an analysis of variance (ANOVA) to quantify the percentage of MUA variance across trials that could be explained by the following task factors: the identity of the cue presented at the beginning of each trial, the task (motion vs. color categorization) to be performed, the motion direction of the categorized stimulus, the color of the categorized stimulus, and the animals' motor choice (left vs. right saccade).

To quantify these types of information we computed a 7-way ANOVA across trials. The first three factors of the ANOVA corresponded to the cue of each trial grouped into two levels according to all three possible pairwise pairings of the four task cues. The first factor corresponded to the cue pairing that reflected the assignment of the cues to the tasks (cross or flower (motion) vs. circle or triangle (color); Fig. 1C). The second and third factors corresponded to the two other cue pairings that did not reflect the cue-task assignment (cross or circle vs. flower or triangle; cross or triangle vs. flower or circle). This construction of these three factors ensured equal statistical properties between factors (balanced number of trials and levels) and fully capturing cue as well as task related spiking variance. Spiking activity that was selective for any or multiple of the four cues yielded non-zero explained variance for any of the three factors. In contrast, spiking activity that was selective for the task (motion vs. color) irrespective of the specific cue yielded non-zero explained variance only for the first of the three factors. Thus, we computed cue information as the average explained variance of all first three factors, and task information as the variance explained by the first factor minus the average variance explained by the second and third factor. The fourth and fifth factor of the ANOVA were the motion direction (7 levels) and color (7 levels) of the stimulus on each trial, respectively. The sixth factor was the choice of the animal on each trial (2 levels, left vs. right). The seventh factor was the choice of the animal on the previous trial (2 levels, left vs. right). Including the choice on the previous trials as a task factor allowed us to quantify choice-predictive

information independent from any potential choice-sequence effects. In other words, we could quantify neuronal information predicting the upcoming choice independent of the last choice.

We quantified neuronal information about each task factor independently. Importantly, the investigated task factors were not orthogonal. E.g., for the motion and color task, motion direction and color were highly correlated with choice, respectively (motion task: $r^2_{\text{motion x choice}} = 0.5$, $r^2_{\text{color x choice}} = 0.002$; color task: $r^2_{\text{motion x choice}} = 0.005$, $r^2_{\text{color x choice}} = 0.5$; all $P < 10^{-16}$ Spearman rank correlation). Thus, we computed an unbalanced ANOVA, that implicitly orthogonalized the different task factors. In other words, we quantified the spiking variance explained be each factor that could not be explained by any of the other factors. E.g., as choice information we measured only the information about the monkeys' choice that was not explained by cue, task, color, motion or the previous choice.

We quantified cue and task information across both tasks. We quantified motion, color and choice information separately for each task (motion vs. color categorization). We then pooled motion, color, and choice information across tasks for several analyses (Figs. 1F, 1H, 2, 3, and 4). If motion and color information is computed across all trials per task, the amount of motion and color information has a different scaling for the motion and color tasks, because both factors have a different correlation with the factor choice depending on the tasks (see correlation statistics above). There is less motion and color information for the corresponding tasks respectively, because there is stronger correlation of these factors with the choice. To rule out this effect for the quantitative comparison of motion and color information between tasks (Fig. 1I), we computed the ANOVA analysis separately for trials from the four quadrants of the stimulus space (Fig. 1B) and both choices. Thus, choices are held constant for each group of trials. We then averaged motion and color information across quadrants and correct choices. To quantify the amount of significantly encoding units (Fig. 1G) we tested for a significant encoding across all trials and both tasks for all types of information.

We estimated the amount of variance explained by each factor ω^2 as

$$\omega^2 = \frac{SS_{Between\ Groups} - df * MSE}{SS_{Total} + MSE}$$

, where $SS_{Between\ Groups} = \sum_{group}^{G} n_{group} * (\bar{x}_{group} - \bar{x})^2$ is the sum of squares between G groups (i.e., levels), $SS_{Total} = \sum_{i}^{N} (x_i - \bar{x})^2$ is the total sum of squares across N trials, $df = G - 1$ are the degrees of freedom, and $MSE = \sum_{i}^{N} (x_i - \bar{x}_{group})^2$ is the mean squared error. ω^2 is an unbiased estimator of explained variance (*35*). In particular, and in contrast to the estimator η^2, ω^2 yields a zero-mean statistic under the Null-hypothesis of no explained variance independent of small sample size N. For each factor of the ANOVA, i.e. for each type of information, we assessed the statistical significance of explained variance

ω^2 using a non-parametric permutation statistic. We compared the measured explained variance to an empirical null-distribution generated by randomly permuting the trial-condition assignment (1000 permutations).

To estimate the time-course of neuronal information, we performed a sliding-window ANOVA shifting a 50 ms window across the trial in 5 ms steps. For all latency estimates, the resulting information time-courses were smoothed with a 50 ms (full width at half maximum) Hanning window. To investigate information dynamics relative to cue and stimulus onset, trials were temporally aligned to stimulus onset (Figs. 2 and 3). To rule out confounds of neuronal information due to the motor response itself in this stimulus-locked analysis, for each trial, we only included neuronal activity up to 5 ms before saccade onset.

To investigate the build-up of choice predictive information before the animals' response, trials were temporally aligned to the choice (saccade onset) (Fig. 4). An important, but typically neglected, caveat for such response-locked analysis is that a difference in average response time between choices can induce spuriously measured choice information. This is because, for different response times between choices, stimulus-locked changes in neuronal activity (e.g., phasic responses to stimulus onset) do not temporally align between choices relative before the response. This temporal misalignment of stimulus-locked changes then leads to erroneously quantifying a difference in neuronal activity as predicting the upcoming choice. To rule out that this confounded choice information, for the response-locked analysis, we equated reaction times between choices by stratification. For each stimulus condition (motion direction, color, and task), we randomly removed trials for both choices to match the response time distributions for both choices. Before stratification, both animals had significantly different reaction times between choices for many stimulus conditions ($p < 0.05$, for 31 and 32 out of 42 motion x color x task conditions). After stratification, no significant differences remained ($p > 0.05$, for both animals and all motion x color x task conditions).

To quantify average amounts of information per region we averaged information time courses across the following time windows (Fig. 1 H and I). Cue and task information: 0.5 s – 1 s post cue (second half of the cue interval); motion and color information: 1.0 s – 1.27 s post cue (stimulus onset to average response latency); choice information: 0.2 s – 0 s pre response (200 ms before response) and -0.5 s – 1 s post cue (pre-stimulus interval).

Information dynamics

We estimated the latency of information as the time at which information reached half its maximum. In contrast to measures based on the time at which information reaches statistical significance, the employed measure is robust to differences in the strength of information or the amount of data. Latencies were not estimated if there was no significant

information ($P > 0.05$) in the interval of interest. This was the case for the transient peak of task information being absent in MT, LIP, PFC and FEF. Furthermore, latencies were not estimated if there was no significant increase (linear regression, $P > 0.05$) of information in the interval of interest. This was the case for pre-response choice information in IT.

Choice information was already significant before stimulus onset in most regions. We ruled out that differences in such pre-stimulus choice information between regions lead to spurious latency differences. To this end, for each region, we subtracted the baseline choice information before estimating half maximum latencies (Fig. 4).

For statistical comparisons of latencies between regions and types of information we estimated the standard error of latencies by bootstrap across units (100 resamples). We then assessed the significance of latency differences using *T*-statistics.

All analysis code was custom written in Matlab and C.

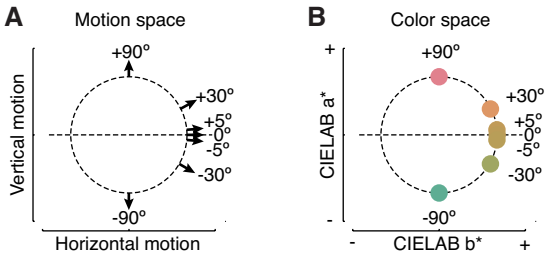

Fig. S1. Stimulus space. Stimuli covered motion direction and color spaces between opposite motion directions (up/down through right) and colors (red/green through yellow). All stimuli were 100% coherent, iso-luminant, and iso-saturated. The circular display illustrates the analogy between both stimulus features. (**A**) Employed motion directions. (**B**) Employed colors. Horizontal dashed lines represent the categorization boundaries.

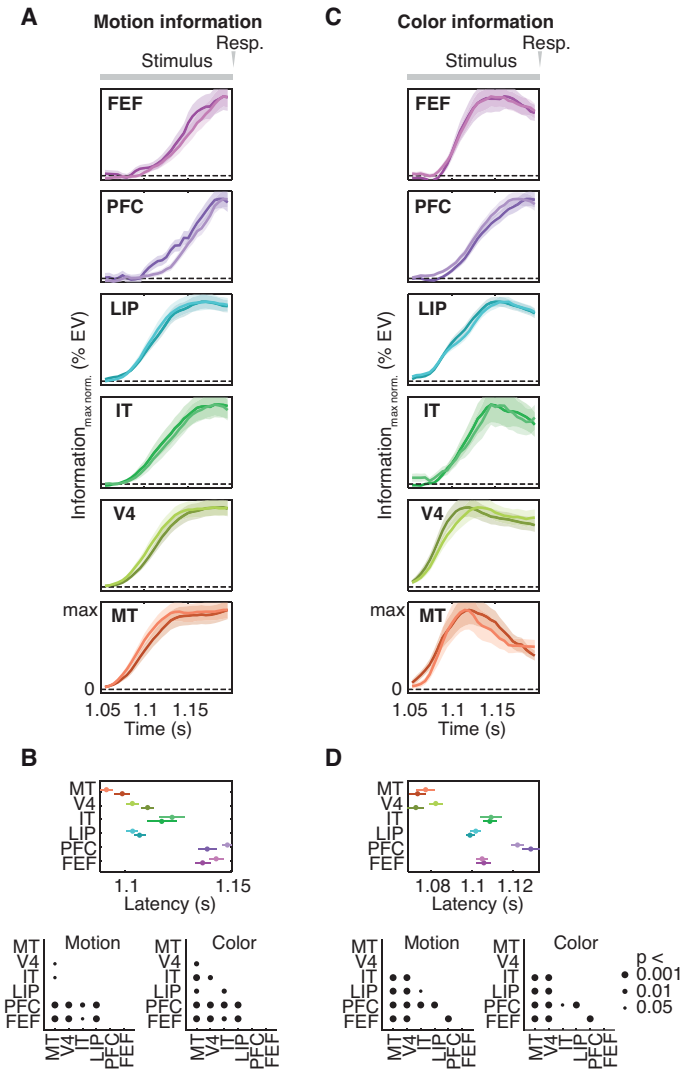

Fig. S2. Dynamics of motion and color information during motion and color categorization tasks. (**A**) Time-courses of neuronal information about motion direction of the categorized stimulus. Panels display time-courses of information normalized by maximum information. (**B**) Comparison of motion information latencies between regions (half maximum information). Black dots in the bottom panels indicate significant latency differences between regions. (**C**) Time-courses of information about the color of the categorized stimulus across regions. Same conventions as in (A). (**D**) Comparison of color information latencies between regions. Same conventions as in (B). All error bars denote SEM. Dark and bright colors correspond to motion and color tasks, respectively.

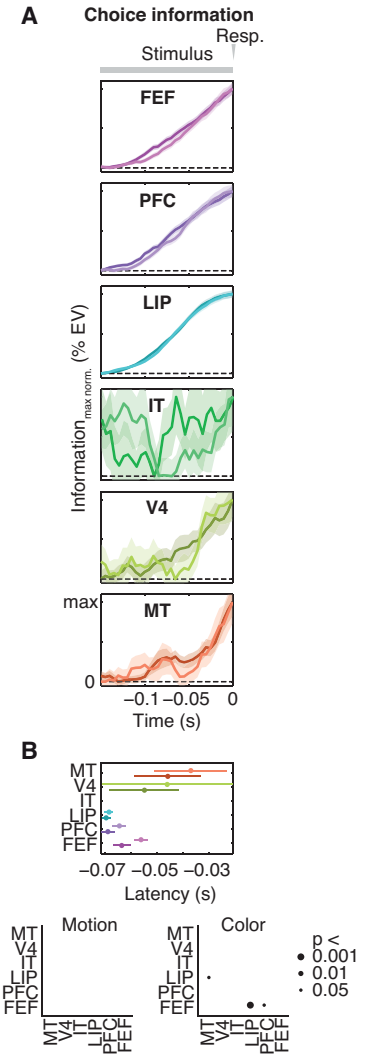

Fig. S3. Dynamics of choice information for motion and color categorization tasks. (**A**) Response locked time-courses of neuronal information about the animas' choice. Panels display information time-courses normalized by maximum information. (**B**) Comparison of stimulus-locked choice information latencies between regions (half maximum information). Black dots in the bottom panels indicate significant latency differences between regions. Latencies were not estimated for IT because there was no significant increase of information in IT in the investigated interval (linear regression, $P > 0.05$). All error bars denote SEM. Dark and bright colors correspond to motion and color task, respectively. There were no significant latency differences for the motion task.

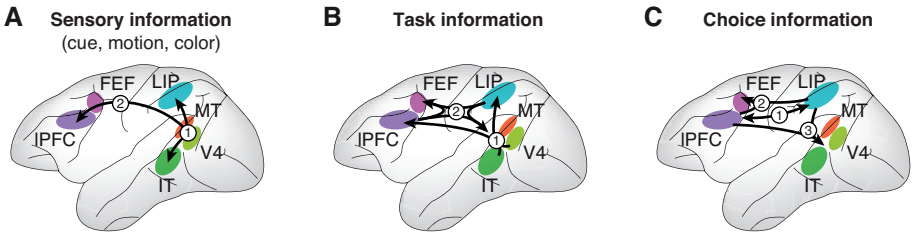

Fig. S4. Schematic information flow during sensorimotor decisions. (**A**) All three types of sensory information (cue, motion, and color) flowed bottom-up from MT and V4, to LIP, IT, FEF and PFC. (**B**) Task information was first extracted in a transient burst in V4 and IT, from where it fed forward to PFC and LIP. Then there was a top-down flow of sustained task information from PFC and LIP to FEF and visual cortex. (**C**) Choice signals simultaneously built up in PFC and LIP. Then choice signals flowed to FEF and visual cortex.

References and Notes

1. D. A. Crowe, S. J. Goodwin, R. K. Blackman, S. Sakellaridi, S. R. Sponheim, A. W. MacDonald 3rd, M. V. Chafee, Prefrontal neurons transmit signals to parietal neurons that reflect executive control of cognition. *Nat. Neurosci.* **16**, 1484–1491 (2013). Medline doi:10.1038/nn.3509

2. S. J. Goodwin, R. K. Blackman, S. Sakellaridi, M. V. Chafee, Executive control over cognition: Stronger and earlier rule-based modulation of spatial category signals in prefrontal cortex relative to parietal cortex. *J. Neurosci.* **32**, 3499–3515 (2012). Medline doi:10.1523/JNEUROSCI.3585-11.2012

3. M. N. Shadlen, W. T. Newsome, Motion perception: Seeing and deciding. *Proc. Natl. Acad. Sci. U.S.A.* **93**, 628–633 (1996). Medline doi:10.1073/pnas.93.2.628

4. D. J. Freedman, J. A. Assad, Experience-dependent representation of visual categories in parietal cortex. *Nature* **443**, 85–88 (2006). Medline doi:10.1038/nature05078

5. C. H. Donahue, D. Lee, Dynamic routing of task-relevant signals for decision making in dorsolateral prefrontal cortex. *Nat. Neurosci.* **18**, 295–301 (2015). Medline doi:10.1038/nn.3918

6. M. G. Stokes, M. Kusunoki, N. Sigala, H. Nili, D. Gaffan, J. Duncan, Dynamic coding for cognitive control in prefrontal cortex. *Neuron* **78**, 364–375 (2013). Medline doi:10.1016/j.neuron.2013.01.039

7. J. N. Kim, M. N. Shadlen, Neural correlates of a decision in the dorsolateral prefrontal cortex of the macaque. *Nat. Neurosci.* **2**, 176–185 (1999). Medline doi:10.1038/5739

8. K. Merten, A. Nieder, Active encoding of decisions about stimulus absence in primate prefrontal cortex neurons. *Proc. Natl. Acad. Sci. U.S.A.* **109**, 6289–6294 (2012). Medline doi:10.1073/pnas.1121084109

9. D. J. Freedman, M. Riesenhuber, T. Poggio, E. K. Miller, Categorical representation of visual stimuli in the primate prefrontal cortex. *Science* **291**, 312–316 (2001). Medline doi:10.1126/science.291.5502.312

10. T. H. Donner, M. Siegel, P. Fries, A. K. Engel, Buildup of choice-predictive activity in human motor cortex during perceptual decision making. *Curr. Biol.* **19**, 1581–1585 (2009). Medline doi:10.1016/j.cub.2009.07.066

11. K. H. Britten, W. T. Newsome, M. N. Shadlen, S. Celebrini, J. A. Movshon, A relationship between behavioral choice and the visual responses of neurons in macaque MT. *Vis. Neurosci.* **13**, 87–100 (1996). Medline doi:10.1017/S095252380000715X

12. H. Nienborg, B. G. Cumming, Decision-related activity in sensory neurons reflects more than a neuron's causal effect. *Nature* **459**, 89–92 (2009). Medline doi:10.1038/nature07821

13. N. K. Logothetis, J. D. Schall, Neuronal correlates of subjective visual perception. *Science* **245**, 761–763 (1989). Medline doi:10.1126/science.2772635

14. J. D. Wallis, K. C. Anderson, E. K. Miller, Single neurons in prefrontal cortex encode abstract rules. *Nature* **411**, 953–956 (2001). Medline doi:10.1038/35082081

15. K. Johnston, H. M. Levin, M. J. Koval, S. Everling, Top-down control-signal dynamics in anterior cingulate and prefrontal cortex neurons following task switching. *Neuron* **53**, 453–462 (2007). Medline doi:10.1016/j.neuron.2006.12.023

16. R. Muhammad, J. D. Wallis, E. K. Miller, A comparison of abstract rules in the prefrontal cortex, premotor cortex, inferior temporal cortex, and striatum. *J. Cogn. Neurosci.* **18**, 974–989 (2006). Medline doi:10.1162/jocn.2006.18.6.974

17. R. Desimone, J. Duncan, Neural mechanisms of selective visual attention. *Annu. Rev. Neurosci.* **18**, 193–222 (1995). Medline doi:10.1146/annurev.ne.18.030195.001205

18. S. Kastner, L. G. Ungerleider, Mechanisms of visual attention in the human cortex. *Annu. Rev. Neurosci.* **23**, 315–341 (2000). Medline doi:10.1146/annurev.neuro.23.1.315

19. J. H. Reynolds, L. Chelazzi, Attentional modulation of visual processing. *Annu. Rev. Neurosci.* **27**, 611–647 (2004). Medline doi:10.1146/annurev.neuro.26.041002.131039

20. V. Mante, D. Sussillo, K. V. Shenoy, W. T. Newsome, Context-dependent computation by recurrent dynamics in prefrontal cortex. *Nature* **503**, 78–84 (2013). Medline doi:10.1038/nature12742

21. J. Duncan, Selective attention and the organization of visual information. *J. Exp. Psychol. Gen.* **113**, 501–517 (1984). Medline doi:10.1037/0096-3445.113.4.501

22. W. Singer, Cortical dynamics revisited. *Trends Cogn. Sci.* **17**, 616–626 (2013). Medline doi:10.1016/j.tics.2013.09.006

23. E. K. Miller, J. D. Cohen, An integrative theory of prefrontal cortex function. *Annu. Rev. Neurosci.* **24**, 167–202 (2001). Medline doi:10.1146/annurev.neuro.24.1.167

24. M. Siegel, T. H. Donner, A. K. Engel, Spectral fingerprints of large-scale neuronal interactions. *Nat. Rev. Neurosci.* **13**, 121–134 (2012). Medline

25. X. J. Wang, Decision making in recurrent neuronal circuits. *Neuron* **60**, 215–234 (2008). Medline doi:10.1016/j.neuron.2008.09.034

26. T. D. Hanks, C. D. Kopec, B. W. Brunton, C. A. Duan, J. C. Erlich, C. D. Brody, Distinct relationships of parietal and prefrontal cortices to evidence accumulation. *Nature* **520**, 220–223 (2015). 10.1038/nature14066 Medline doi:10.1038/nature14066

27. K. Wimmer, A. Compte, A. Roxin, D. Peixoto, A. Renart, J. de la Rocha, Sensory integration dynamics in a hierarchical network explains choice probabilities in cortical area MT. *Nat. Commun.* **6**, 6177 (2015). Medline doi:10.1038/ncomms7177

28. M. Siegel, K. P. Körding, P. König, Integrating top-down and bottom-up sensory processing by somato-dendritic interactions. *J. Comput. Neurosci.* **8**, 161–173 (2000). Medline doi:10.1023/A:1008973215925

29. N. K. Logothetis, J. Pauls, M. Augath, T. Trinath, A. Oeltermann, Neurophysiological investigation of the basis of the fMRI signal. *Nature* **412**, 150–157 (2001). Medline doi:10.1038/35084005

30. T. van Kerkoerle, M. W. Self, B. Dagnino, M. A. Gariel-Mathis, J. Poort, C. van der Togt, P. R. Roelfsema, Alpha and gamma oscillations characterize feedback and feedforward

processing in monkey visual cortex. *Proc. Natl. Acad. Sci. U.S.A.* **111**, 14332–14341 (2014). Medline doi:10.1073/pnas.1402773111

31. W. F. Asaad, N. Santhanam, S. McClellan, D. J. Freedman, High-performance execution of psychophysical tasks with complex visual stimuli in MATLAB. *J. Neurophysiol.* **109**, 249–260 (2013). Medline doi:10.1152/jn.00527.2012

32. W. F. Asaad, E. N. Eskandar, A flexible software tool for temporally-precise behavioral control in Matlab. *J. Neurosci. Methods* **174**, 245–258 (2008). Medline doi:10.1016/j.jneumeth.2008.07.014

33. S. Barash, R. M. Bracewell, L. Fogassi, J. W. Gnadt, R. A. Andersen, Saccade-related activity in the lateral intraparietal area. I. Temporal properties; comparison with area 7a. *J. Neurophysiol.* **66**, 1095–1108 (1991). Medline

34. C. J. Bruce, M. E. Goldberg, Primate frontal eye fields. I. Single neurons discharging before saccades. *J. Neurophysiol.* **53**, 603–635 (1985). Medline

35. S. Olejnik, J. Algina, Generalized eta and omega squared statistics: Measures of effect size for some common research designs. *Psychol. Methods* **8**, 434–447 (2003). Medline doi:10.1037/1082-989X.8.4.434